IOP Publishing Physica Scripta
Phys. Scr. 95 (2020) 045801 (5pp) https://doi.org/10.1088/1402-4896/ab5b45

Linear and nonlinear susceptibilities in $GaN/Al_xGa_{1-x}N$ quantum wire

N Zeiri[1,3], A. Bouazra[1], S Abdi-Ben Nasrallah[2] and M Said[1]

[1] Laboratoire de la Matière Condensée et des Nanosciences (LMCN) Département de Physique, Faculté des Sciences de Monastir, 5019 Monastir, Tunisia
[2] Laboratoire d'Etudes des Systèmes Thermique et Energétique (LESTE), Université de Monastir, Tunisia

E-mail: zeirinabil@gmail.com

Received 6 September 2019, revised 9 November 2019
Accepted for publication 25 November 2019
Published 11 February 2020

Abstract

In this work, we have performed a new approach based on a combination of coordinate transformation and the finite difference method in order to investigate the electronic, linear and nonlinear optical properties of $GaN/Al_xGa_{1-x}N$ quantum wire. The real and the imaginary parts of first-order linear and third-order nonlinear susceptibilities are investigated as a function of the quantum wire height and Aluminum mole fraction. Our calculations revealed that as the height increases, the transition energy decreases monotonically. In addition, the peaks of susceptibility decreased and shifted to the red as the height augments. Our findings can serve the experimental studies linked to practical exploitation of the quantum confinement effect in optoelectronic devices based on quantum wire nanostructures.

Keywords: nonlinear optic, quantum wire, coordinate transformation, optical susceptibility

(Some figures may appear in colour only in the online journal)

1. Introduction

Over the last two decades, physical properties of quantum wells, quantum wires and quantum dots have attracted the interest of theoretical and experimental investigations [1–8]. These nanostructures exhibit new electronic and optical properties offering a wide range of potential applications in optoelectronic devices, photodetectors [9, 10], far-infrared laser amplifiers [11, 12], light emitting diodes [13, 14] and solar cells [15]. Thanks to the molecular beam epitaxy technique [16–18], it has become possible to synthesize a certain type of cross-sections such as dome, lens shaped, T-shaped [19], elliptical [20] and V-groove quantum wires [21–24]. The accessibility of controlled manipulation of single-electron energie in quantum wire through effective radius, electric/magnetic fields and spin–orbit interactions has stimulated an excessive activity in the study of both electronic and optical properties [25, 26]. Recently, many works have been reported on quantum wires [27–33]. Authors of [27] studied the effect of electric and magnetic field on the linear, the third-order nonlinear and the total optical absorption coefficient (OAC) for GaAs/AlGaAs quantum wire and they found that the magnitude of OAC is ameliorated in presence of electric field. Tshipa *et al* [29] discussed the donor impurity binding energies of $GaAs/Al_xGa_{1-x}As$ cylindrical quantum wires. Their results depicted that the binding energy augments with the increase of the parallel external magnetic field. In [30] authors have reported a theoretical study of the optical properties for $InAs/In_{0.5}Al_{0.48}As$ quantum wire subjected to an inclined transverse electric field. They have demonstrated that the optical properties are strongly affected by the direction and the strength of the applied electric field. In 2013, Sonawane *et al* [33] investigated the electron confinement in $GaN/Al_xGa_{1-x}N$ quantum wire for different wire widths and aluminum mole fraction. Their analysis showed that spread of electron confinement is reduced with an increase in aluminum composition in the barrier.

In this work, we present a detailed study of electronic and optical properties for $GaN/Al_xGa_{1-x}N$ quantum wire. The linear and the third order nonlinear optical susceptibilities are discussed. The two dimensional Schrödinger equation is resolved in order to determine wave functions and state energies of charge carriers. Theoretical analyses are presented on the base of these numerical calculations as follows. In

[3] Author to whom any correspondence should be addressed.

section 2, we give some details of the coordinate transformation steps and the theoretical model. The results and a conclusion will be presented in sections 3 and 4 respectively.

2. Theoretical model and coordinate transformation

The model of the coordinate transformation have been used in our latest works for modelling quantum wires and dots [34, 35] and gives a good results, compared with experimental data. We present in this part, a bref detail of the mathematical method and we start with the 2D Schrödinger equation:

$$\frac{-\hbar^2}{2}\left(\frac{\partial}{\partial x}\frac{1}{m^*_{x,y}}\frac{\partial\psi(x,y)}{\partial x}+\frac{\partial}{\partial y}\frac{1}{m^*_{x,y}}\frac{\partial\psi(x,y)}{\partial y}\right)+\left[\frac{\hbar^2k_z^2}{2m^*}+U_p(x,y)=E\psi(x,y)\right], \quad (1)$$

where m^* is the electron or hole effective mass, $U_p(x, y)$ is the 2D potential profile determined by the conduction band offset.

The general coordinate transformations used in this work are $x = x(u, v)$ and $y = y(u, v)$ and the Schrödinger equation, given by equation (1) in the old coordinate space $\varepsilon = \varepsilon(x, y)$, can be mapped into the new space $\beta = \beta(u, v)$ as:

$$\begin{aligned}\frac{-\hbar^2}{2}\Bigg[&u_x\frac{\partial}{\partial u}\left(\frac{u_x}{m^*}\frac{\partial\psi}{\partial u}+\frac{v_x}{m^*}\frac{\partial\psi}{\partial v}\right)\\&+v_x\frac{\partial}{\partial u}\left(\frac{u_x}{m^*}\frac{\partial\psi}{\partial u}+\frac{v_x}{m^*}\frac{\partial\psi}{\partial v}\right)\\&+u_y\frac{\partial}{\partial u}\left(\frac{u_y}{m^*}\frac{\partial\psi}{\partial u}+\frac{v_y}{m^*}\frac{\partial\psi}{\partial v}\right)\\&+v_y\frac{\partial}{\partial v}\left(\frac{u_y}{m^*}\frac{\partial\psi}{\partial u}+\frac{v_y}{m^*}\frac{\partial\psi}{\partial v}\right)\Bigg]+U\psi=E\psi. \quad (2)\end{aligned}$$

In equation (2), $\psi[x(u, v), y(u, v)] = \psi(u, v)$, $U_p[x(u, v), y(u, v)] = U_p(u, v)$ while u_x, u_y, v_x and v_y are the elements of the Jacobian matrix $J_{x,y}$ representing partial derivatives of the inverse functions $u = u(x,y)$ and $v = v(x,y)$ with respect to x and y. The calculations are detailed in [30].

The linear and nonlinear susceptibilities can be calculated using the quantum density matrix formalism [36].

The first order linear and third order non linear susceptibilities are given by [37]:

$$\chi^{(1)}(\omega)=\frac{\sigma}{\hbar\varepsilon_0}\frac{|M_{ij}|^2}{(\omega|fi-\omega-\mathrm{i}\gamma_{fi})} \quad (3)$$

and

$$\chi^{(3)}(\omega)=\frac{\sigma}{\hbar^3\varepsilon_0}\frac{|M_{ij}|^2}{(\omega_{fi}-\omega-\mathrm{i}\gamma_{fi})}\times\left\{\frac{4\,|M_{ij}|^2}{(\omega_{fi}-\omega)^2+\gamma_{fi}^2}-\frac{(M_{ff}-M_{ii})^2}{(\omega_{fi}-\mathrm{i}\gamma_{fi})(\omega_{fi}-\omega-\mathrm{i}\gamma_{fi})}\right\}, \quad (4)$$

where M_{ij} is the transition dipole moment defined by:

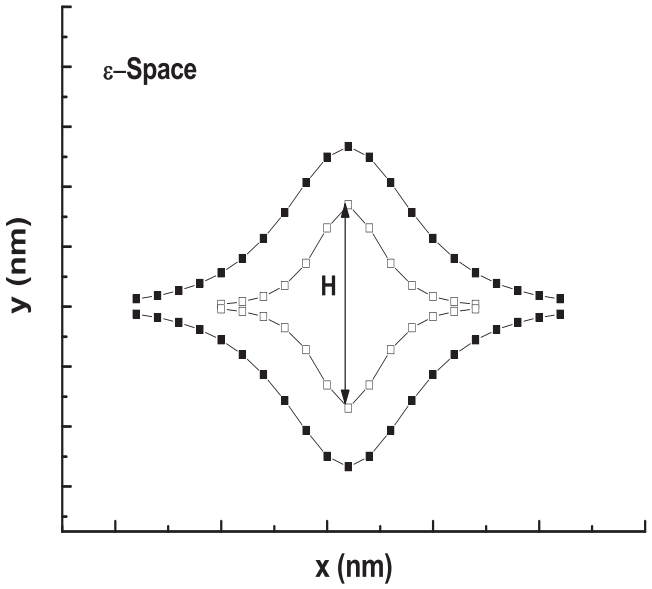

Figure 1. The cross-section profile of GaN/$Al_xGa_{1-x}N$ quantum wire

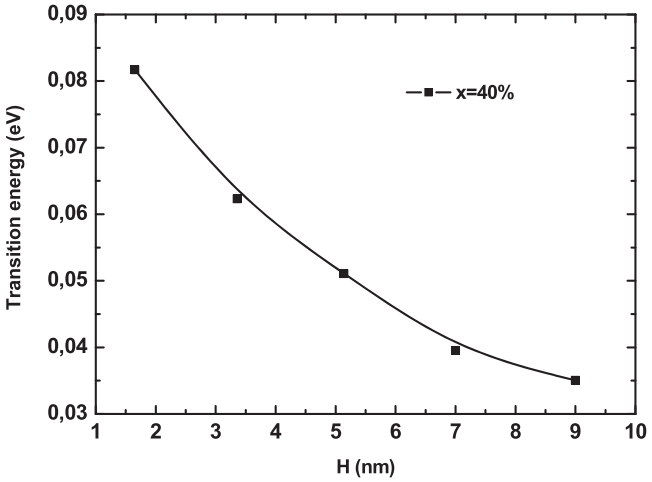

Figure 2. The transition energy ΔE as a function of the quantum wire height H for a given mole fraction of Aluminum $x = 40\%$.

$M_{ij} = \psi_f|-er|\psi_i$ and $\omega_{fi} = (E_f - E_i)/\hbar$ is the corresponding transition angular frequency between two states. σ represents the charge carrier density and γ_{ij} is the damping rate and $\mu_{if} = M_{ff} - M_{ii}$ is the geometrical factor.

3. Results and discussion

The shape of the quantum wire structure shown in figure 1 and the different material parameters used in our numerical work are taken from [38]: $E_g(\mathrm{GaN}) = 3.29$ eV. The effective mass of GaN and $Al_xGa_{1-x}N$ are $m^*_{\mathrm{GaN}} = 0.19m_0$ and $m^*_{Al_xGa_{1-x}N} = (0.19(1-x) + 0.33)m_0$. We have taken V_c (GaN/$Al_xGa_{1-x}N$) $= 0.75(E_g(x)–E_g(0))$ [39], $\sigma = 5 \times 10^{16}$ cm^{-3}, while x is taken equal to 0.4 in this part.

In figure 2 the transition energy ΔE is displayed as a function of the quantum wire height H for a given mole

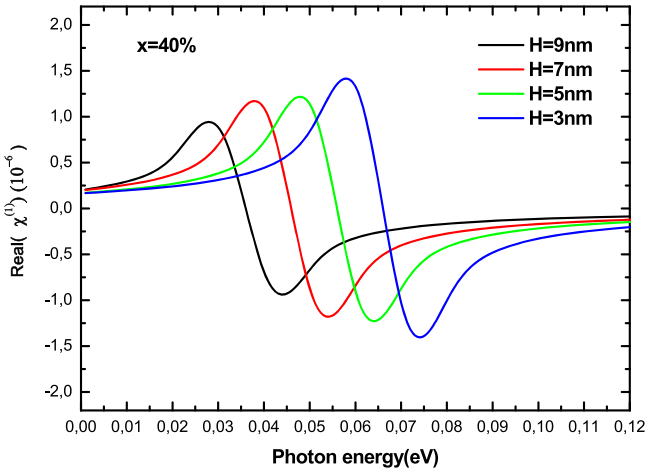

Figure 3. The real (Real$\chi^{(1)}$) part of the first linear susceptibility as a function of pump photon energy $\hbar\omega$ (eV) for different values of height H while $x = 40\%$.

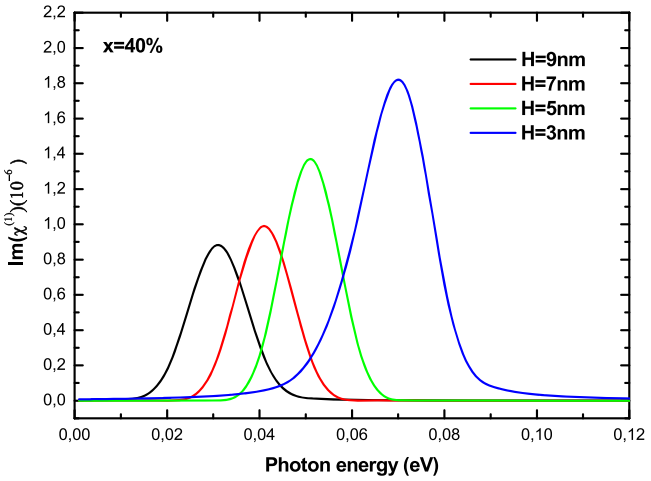

Figure 4. The imaginary (Im$\chi^{(1)}$) part of the first linear susceptibility as a function of pump photon energy $\hbar\omega$ (eV) for different values of height H while $x = 40\%$.

fraction of Aluminum ($x = 0.4$). One can easily remark that ΔE decreases monotonically as H increases. For example if $H = 7$ nm, $\Delta E \approx 0.04$ eV. For larger values of H, the transition energy will further decrease and tend towards zero. This can be related to quantum confinement effect when enlarging H, interval distance between states becomes more reduced. These findings have been reported in many [33, 36, 40].

In figure 3, the Real$\chi^{(1)}$ has been plotted as a function of pump photon energy $\hbar\omega$(eV) for different values of height H while $x = 40\%$. As can be seen from this figure, the effect of increasing H gives a spectacular decrease of the magnitude and a very rapid shift of the susceptibility peak toward the longer wavelengths. According to figure 3, we can underline the fact that the magnitude of Real$\chi^{(1)}(\omega)$ is around 10^{-6}. For bigger height ($H = 9.0$ nm), the intensity of Real$\chi^{(1)}$ diminishes and switches from -0.9×10^{-6} to $+0.9 \times 10^{-6}$ near 0.035 eV. Our results are in a good agreement with those of [36] where analysis revealed that Real$\chi^{(1)}(\omega)$ changes its sign near the resonant frequency (80 meV).

In figure 4, the Im$\chi^{(1)}(\omega)$ has been displayed as a function of pump photon energy $\hbar\omega$(eV) for different values of height H while $x = 40\%$. From the plot one can confirm that the imaginary part of first order linear susceptibility is strongly influenced by H change. In addition, with the increase of H, peaks of Im$\chi^{(1)}(\omega)$ are reduced and red shifted. For example, if we select $H = 9.0$ nm, the peak of Im$\chi^{(1)}(\omega)$ has reached the value 0.88×10^{-6} and is approximately located at 0.03 eV.

The impact of quantum wire height H on real (Real$\chi^{(3)}(\omega)$) part of third order nonlinear susceptibility has been illustrated as a function of pump photon energy $\hbar\omega$ (eV) for a given Aluminum mole fraction $x = 40\%$ in figure 5. As can be seen from the figure, the augmentation of H is followed on the one hand by a remarkable decrease in the amplitude of susceptibility and in the other hand by a significant shift of the peaks towards the low frequencies. The

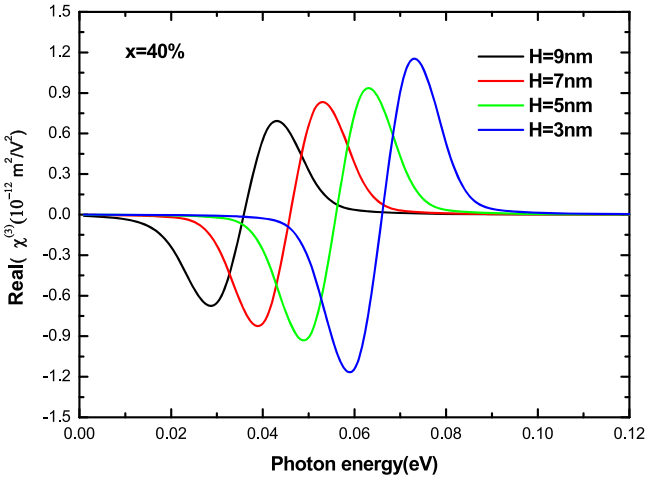

Figure 5. The real (Real$\chi^{(3)}$) part of the third order nonlinear susceptibility as a function of pump photon energy $\hbar\omega$ (eV) for a given aluminum mole fraction $x = 40\%$.

magnitude of Real$\chi^{(3)}(\omega)$ is $10^{-12}\,\mathrm{m^2\,V^{-2}}$. This can be attributed to quantum confinement effect [41].

The result of the imaginary part of the third order nonlinear susceptibility (Im$\chi^{(3)}$) has been pictured in figure 6 as a function of pump photon energy $\hbar\omega$ (eV) for different values of quantum wire height H while $x = 40\%$. From the plot, it is obvious to observe that the Im$\chi^{(3)}$ keeps always a negative value and decreases when H augments. For $H = 3.0$ nm, the peak of Im$\chi^{(3)}$ is equal to $-1.52 \times 10^{-12}\,\mathrm{m^2\,V^{-2}}$ and situated at 0.07 eV. The same behavior is obtained in comparison with figure 4 where peaks of Im$\chi^{(3)}(\omega)$ are witnessing a red shift. The results of this study are necessary in designing polarization-sensitive photo-detectors [42, 43] and telecommunications [44, 45].

The susceptibility is related to the geometrical factor $|\mu_{if}|$ which is strongly affected by the height H. In fact, the quantum confinement effect due to the decrease of H, intensifies the peaks of susceptibilities.

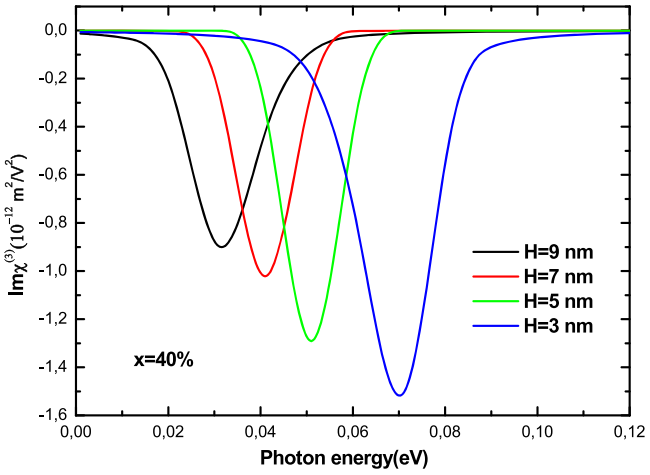

Figure 6. The imaginary ($\mathrm{Im}\chi^{(3)}$) part of the third order nonlinear susceptibility as a function of pump photon energy $\hbar\omega$ (eV) for different values of quantum wire height H while $x = 40\%$.

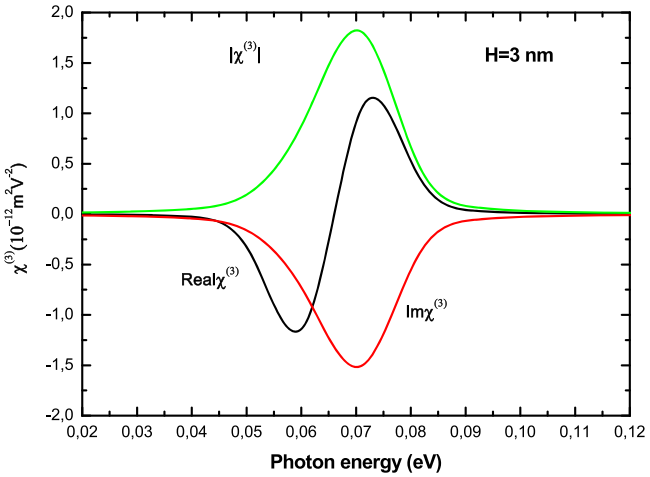

Figure 7. The Real$\chi^{(3)}$, Im$\chi^{(3)}$ and $|\chi^{(3)}|$ as a function of pump photon energy $\hbar\omega$ (eV) for a fixed quantum wire height $H = 3.0$ nm.

In figure 7, Real $\chi^{(3)}(\omega)$, Im$\chi^{(3)}(\omega)$ and $|\chi^{(3)}(\omega)|$ have been illustrated as a function of pump photon energy $\hbar\omega$ (eV) for a selected quantum wire height ($H = 3.0$ nm). The plot indicates that $|\chi^{(3)}(\omega)| = 1.81 \times 10^{-12}\,\mathrm{m^2\,V^{-2}}$ while Real$\chi^{(3)}(\omega)$ changes it signs from $-1.15 \times 10^{-12}\,\mathrm{m^2\,V^{-2}}$ to $+1.15 \times 10^{-12}\,\mathrm{m^2\,V^{-2}}$ at 0.07 eV. These particular values of the susceptibility obtained in our theoretical model opens the access for the design of the optoelectronic devices which requires weak transition energies. This conclusion has been mentioned in [27].

In figure 8, we have depicted the maximum of imaginary part of first order linear and third order nonlinear susceptibility as a function of different values of height H while $x = 40\%$. It is worthy to underline the influence of varying H on the $\chi_{\max}$. In fact, increasing H has reduced dramatically the maximum of both Im$\chi^{(1)}$ and Im$|\chi^{(3)}|$. For $H = 8.0$ nm, the maximum of Im$\chi^{(1)} = 0.94 \times 10^{-6}\,\mathrm{m^2\,V^{-2}}$ while it is equal to $0.96 \times 10^{-12}\,\mathrm{m^2\,V^{-2}}$ for Im$|\chi^{(3)}|$. Our findings can be at the service of diverse fields of quantum wires such as quantum electronics [46, 47] and nonlinear optics [48–50].

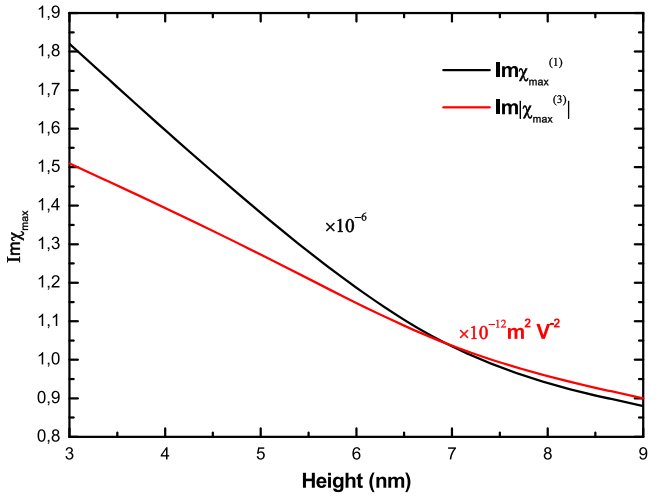

Figure 8. The maximum of the imaginary part of the first order linear and third order nonlinear susceptibility as a function of different values of height H while $x = 40\%$.

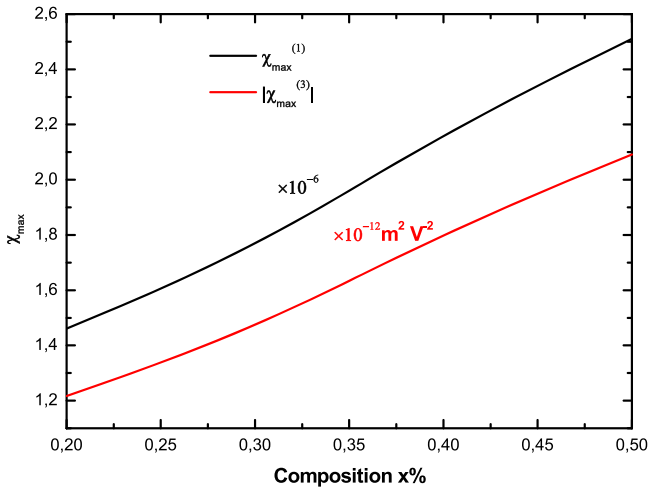

Figure 9. The maximum of the first order linear and modulus of third order nonlinear susceptibility as a function of different values of Aluminum mole fraction while $H = 3.0$ nm.

Figure 9 reflects the maximum of the first order linear and modulus of third order nonlinear susceptibility for different Aluminum mole fraction x with a fixed height $H = 3.0$ nm. A great enhancement in the amplitude of susceptibility is obtained when x is increased. It should be noted here that for $x = 40\%$ the magnitude of third order nonlinear susceptibility (figure 9) is around $1.80 \times 10^{-12}\,\mathrm{m^2\,V^{-2}}$. Several studies examining the the importance of nonlinear susceptibility for optical switching device have been published recently [51, 52].

In reference [52], Liua *et al* have studied, using the effective mass approximation, the tuning of linear and nonlinear optical absorption in laterally coupled $Al_xGa_{1-x}As/GaAs$ quantum wires. They found that, by decreasing the gap, the linear and nonlinear absorption coefficient displayed a blue shift. In [53], authors have evaluated the nonlinear optical rectification in laterally-coupled quantum well wires with applied electric filed, using the

effective mass formalism. Their result showed that χ_0^2 is strongly influenced by the external electric field.

4. Conclusions

In this work, a new numerical method based on a combination of coordinate transformation has been presented in detail in order to model GaN/$Al_xGa_{1-x}N$ quantum wire. Our interest has focused on the study of the real and the imaginary part of first-order linear and third-order nonlinear optical susceptibilities as a function of two major factors: height H and aluminum composition x. Calculations depicted that the transition energy ΔE diminishes rapidly as H rises. In addition, peaks of susceptibility are reduced and redshifted when H is enlarged. Results depicted that by increasing Aluminum mole fraction, amplitude of susceptibility is ameliorated for both linear and nonlinear terms. The results of this work can represent a great contribution in technological applications where quantum wires are required.

ORCID iDs

N Zeiri https://orcid.org/0000-0003-3050-8262

References

[1] Vaseghi B, Khordad R and Golshan M M 2006 *Phys. Status Solidi* B **243** 2772
[2] Kasapoglu E, Ungan F, Sari H and Sokmen I 2009 *Superlattices Microstruct.* **45** 618–23
[3] Khordad R and Khaneghah S K 2011 *Phys. Status Solidi* B **248** 243–49
[4] Pershin Y V, Nesteroff J A and Privman V 2004 *Phys. Rev.* B **69** 121306
[5] Zhang S, Liang R, Zhang E, Zhang L and Liu Y 2006 *Phys. Rev.* B **73** 155316
[6] Zeiri N, Naifar A, Abdi-Ben Nasrallah S and Said M 2018 *Optik* **176** 162–67
[7] Naifar A, Zeiri N, Abdi-Ben Nasrallah S and Said M 2017 *Optik* **146** 90–7
[8] Namvari E, Shojaeia S and Asgari A 2017 *Superlattices Microstruct.* **112** 118–27
[9] Nasr A 2009 *Opt. Laser Technol.* **41** 871–76
[10] Das B and Singaraju P 2005 *Infrared Phys. Technol.* **46** 209–18
[11] Reithmaier J P, Somers A, Deubert S, Schwertberger R, Kaiser W, Forchel A and Tromborg B 2005 *Appl. Phys.* D **38** 2088
[12] Saravanan S, Peter A J and Lee C W 2016 *Eur. Phys. J.* D **70**
[13] Minot E D, Kelkensberg F, van Kouwen M, van Dam J A, Kouwenhoven L P, Zwiller V and Bakkers E P A M 2007 *Nano Lett.* **7** 367–71
[14] Pescaglini A, Gocalinska A, Bogusevschi S, Moroni S T, Juska G, Mura E E and Pelucchi E 2018 *ACS Photonics* **5** 1318–25
[15] Kunets V P, Furrow C S, Morgan T A, Hirono Y, Ware M E, Dorogan V G and Salamo G J 2012 *Appl. Phys. Lett.* **101** 041106
[16] Fujikura H, Muranaka T and Hasegawa H 1999 *Microelectron. J.* **30** 397–401
[17] Nötzel R, Gong Q, Ramsteiner M, Jahn U, Friedland K and Ploog K 2002 *Microelectron. J.* **33** 573–8
[18] Eberl K, Grambow P, Lehmann A, Kurtenbach A, Klitzing K V, Heitmann D and Hohenstein M 1993 *Appl. Phys. Lett.* **63** 1059
[19] Akiyana H, Yoshita M, Pfeiffer L N, West K W and Pinczuk A 2003 *App. Phys. Lett* **82** 379
[20] Van den Broek M and Peeters F M 2001 *Physica* E **11** 345–55
[21] Khordad R, KheiryzadehKhaneghah S and Masoumi M 2010 *Superlattices Microstruct.* **47** 538–49
[22] Gvozdic D M and Schalachetzki A 2002 *J. Appl. Phys* **92** 2023
[23] Dwir B, Utke I, Kaufman D and Kapon E 2000 *Microelectron. Eng.* **53** 295–8
[24] Palmgren S, Weman H, Schoenberg A, Karlsson K F, Dupertuis M A, Leifer K and Kapon E 2006 *Appl. Phys. Lett.* **89** 191111
[25] Zhang Y-Y and Yao G-R 2011 *J. Appl. Phys.* **110** 093104
[26] Sugaya T, Jang K-Y, Hahn C-K, Ogura M, Komori K, Shinoda A and Yonei K 2005 *J. Appl. Phys.* **97** 034507
[27] Karimi M J and Hosseini M 2017 *Superlattices Microstruct.* **111** 96–102
[28] Nag S and Bhattacharya D P 2019 *Physica* E **106** 78–84
[29] Tshipa M, Winkoun D P, Nijegorodov N and Masale M 2018 *Superlattices Microstruct.* **116** 227–37
[30] Bouazra A, Abdi-Ben Nasrallah S and Said M 2017 *Optik* **147** 328–33
[31] Dey A W, Svensson J, Ek M, Lind E, Thelander C and Wernersson L E 2013 *Nano Lett.* **13** 5919–24
[32] Ballicchia M, Weinbub J and Nedjalkov M 2018 *Nanoscale* **10** 23037–49
[33] Sonawane U S, Samuel E P, Zope U and Patil D S 2013 *Optik* **124** 802–6
[34] Bouazra A, Abdi-Ben Nasrallah S and Said M 2016 *Physica* E **75** 272–9
[35] Bouazra A, Mnasri S, Abdi-Ben Nasrallah S and Said M 2014 *Comput. Phys. Commun.* **185** 1290–8
[36] Shahzadeh M and Sabaeian M 2014 *AIP Adv.* **4** 067113
[37] Sabaeian M and Shahzadeh M 2015 *Physica* E **68** 215–23
[38] Abouelaoualim D, Elkadadra A, Oueriagli A and Outzourhit A 2012 *J. Nano-Electron. Phys.* **4** 03004
[39] Xie W 2011 *Opt. Commun.* **284** 1872–5
[40] Zaouali F, Bouazra A and Said M M 2018 *Optik* **158** 541–7
[41] Feng X, Xiong G, Zhang X and Gao H 2006 *Physica* B **383** 207–12
[42] Singh A *et al* 2007 *Nano Lett.* **7** 2999–3006
[43] Yu Y, Protasenko V, Jena D, Xing H G and Kuno M 2008 *Nano Lett.* **8** 1352–7
[44] Saravanan S and Peter A J 2015 *Mater. Today: Proc.* **2** 4373–7
[45] Usman M *et al* 2011 *J. Appl. Phys.* **109** 104510
[46] Kim R and Ludstrom M 2008 *IEEE Trans. Nanotechnol.* **7** 787–94
[47] Neophytou N, Paul A, Lundstrom M S and Klimeck G 2008 *IEEE Trans. Electron Devices* **55** 1286–97
[48] Huang W, Xu M and Jain F 2001 *Int. J. Infrared Millim. Waves* **22** 1009–18
[49] Lytel R, Mossman S M and Kuzyk M G 2015 *Opt. Lett.* **40** 4735–8
[50] Wang G 2005 *Phys. Rev. B* **72** 155329
[51] Hasanirokh K, Asgari A and Mahdizadeh Rokhi M 2019 *Optik* **188** 99–103
[52] Liu G, Guo K, Xie L, Zhang Z and Lu L 2018 *J. Alloys Compd.* **743** 746–55
[53] Liu G, Guo K, Xie L, Zhang Z, Hassanadi H and Lu L 2017 *Superlattices Microstruct.* **103** 230–44